



## The effect of the synthesis conditions on structure and photocatalytic activity of Nb<sub>2</sub>O<sub>5</sub> nanostructures

Caterine Daza Gómez<sup>1</sup>, Jorge Enrique Rodríguez-Páez<sup>2,\*</sup>

<sup>1</sup>Departamento de Química, Universidad del Cauca, Cauca, Colombia

<sup>2</sup>Departamento de Física, Universidad del Cauca, Grupo de investigación en Ciencia y Tecnología de Materiales Cerámicos (CYTEMAC), Cauca, Colombia

Received 8 February 2018; Received in revised form 31 July 2018; Accepted 10 August 2018

### Abstract

In this work, niobium pentoxide (Nb<sub>2</sub>O<sub>5</sub>) nanoparticles of varying sizes and morphology were synthesized using the controlled precipitation method. Ammonium niobate oxylate hydrate (NH<sub>4</sub>)<sub>2</sub>[NbO(C<sub>2</sub>O<sub>4</sub>)<sub>3</sub>] · 3 H<sub>2</sub>O was used as a niobium precursor and distilled water or acetic acid was used as solvent. The obtained solids were characterized using Fourier transform infrared and Raman spectroscopies, X-ray diffraction and transmission electron microscopy. The as-synthesized solid precipitate was amorphous, but after heat treatment between 500 °C and 600 °C, the T-Nb<sub>2</sub>O<sub>5</sub> phase was obtained. The size of the primary particles of the niobium pentoxide was nanometric (<100 nm), with agglomerate size of >500 nm, when water was used as a solvent for synthesis. Considering the nature of the process, a possible reaction mechanism of the precursor with the water and NH<sub>4</sub>OH was proposed, which explains the formation of the solid within an aqueous solution. Considering one potential use of Nb<sub>2</sub>O<sub>5</sub> synthesized in this work, the photo-degradation action of the particles on the organic molecule methylene blue was tested. The sample synthesized in acetic acid at pH ~9.0 and heat treated at 600 °C showed the highest photo-degradation capacity, with a degradation of ~60% of the dye for 60 minutes.

**Keywords:** synthesis, niobium pentoxide, controlled precipitation, formation mechanism, photo-degradation

### I. Introduction

Niobium pentoxide (Nb<sub>2</sub>O<sub>5</sub>) and its compounds are of great technological interest due to the physical and chemical properties that they exhibit. These make them useful in applications such as optical and electrochromic devices [1–3], gas sensors [4–6], microelectronics and as catalysts [7,8]. Generally, it exhibits high activity in acid-catalysed reactions in which water molecules are involved [9,10], such as hydration, etherification, hydrolysis, condensation, alkylation, dehydrogenation and especially in oxidation reactions [11]. As niobium is a transition element, it reacts with oxygen encouraging the formation of different stoichiometric oxides, including NbO, Nb<sub>2</sub>O<sub>3</sub>, NbO<sub>2</sub> and Nb<sub>2</sub>O<sub>5</sub> [8]. Nb<sub>2</sub>O<sub>5</sub> is the best known and most studied due to, among other characteristics, its nature as an n-type semiconductor.

The different polymorphic forms of Nb<sub>2</sub>O<sub>5</sub> include TT-Nb<sub>2</sub>O<sub>5</sub> (pseudo-hexagonal), T-Nb<sub>2</sub>O<sub>5</sub> (orthorhombic) and H-Nb<sub>2</sub>O<sub>5</sub> (monoclinic), which are the most common [12,13]. H-Nb<sub>2</sub>O<sub>5</sub> is the most thermodynamically stable, whereas TT-Nb<sub>2</sub>O<sub>5</sub> the least stable. Thus, it is possible to convert the amorphous niobic acid to TT-Nb<sub>2</sub>O<sub>5</sub> at low temperature, transforming itself to T-Nb<sub>2</sub>O<sub>5</sub> by heating between 600 °C and 800 °C and to H-Nb<sub>2</sub>O<sub>5</sub> at approximately 1100 °C [8,14,15]. The different crystalline phases of Nb<sub>2</sub>O<sub>5</sub> can be described considering [NbO<sub>6</sub>] octahedra or pentagonal bi-pyramids arranged in different ways. Therefore, the different crystalline phases of Nb<sub>2</sub>O<sub>5</sub> are formed as 3D structures of distorted [NbO<sub>6</sub>] units, with some [NbO<sub>7</sub>] and [NbO<sub>8</sub>] sites in the TT and T phases. This wealth of structural isotropy brings about the different physicochemical properties of Nb<sub>2</sub>O<sub>5</sub>, including its electronic, electrochromic, sensor, magnetic and electrical properties. Additionally, the catalytic and photocatalytic properties, as well as its surface acidity, are also linked to these structural characteristics and the existence of intrinsic defects.

Nb<sub>2</sub>O<sub>5</sub> has been synthesized using different pro-

\*Corresponding authors: tel: +57 28209800,  
e-mail: [jnpaez@unicauca.edu.co](mailto:jnpaez@unicauca.edu.co)

cesses [16–19], among them sol-gel method [20,21] and hydrothermal process [22]. Lopes *et al.* [23] synthesized Nb<sub>2</sub>O<sub>5</sub> nanoparticles by the oxidant-peroxo method (OPM). The obtained solids showed a mixture of Nb<sub>2</sub>O<sub>5</sub> · nH<sub>2</sub>O and T-Nb<sub>2</sub>O<sub>5</sub> phases, with different morphologies and particle sizes. In addition, they showed the efficiency of the synthesized Nb<sub>2</sub>O<sub>5</sub> in the degradation of Rhodamine B. Meanwhile, Rodrigues and da Silva [24] obtained Nb<sub>2</sub>O<sub>5</sub> · 3 H<sub>2</sub>O nanoparticles with spherical morphology and specific surface area of 60 m<sup>2</sup>/g using water/heptane/CTAB as the reaction medium.

A specific application of Nb<sub>2</sub>O<sub>5</sub>, or compounds of niobium, is related to the heterogeneous photocatalysis, specifically to the removal of organic and inorganic contaminants, with the generation of hydrogen [25,26]. Semiconductors, such as Nb<sub>2</sub>O<sub>5</sub>, might be used, through heterogeneous photocatalysis, for environmental remediation that have shown significant advantages over conventional technologies, allowing the degradation of organic pollutants into innocuous end products [25,27]. The irradiation of the semiconductor with a suitable radiation source, typically in the UV or preferably in the visible region, frequently generates electron-hole pairs [28]. A portion of these electron-hole pairs diffuse to the surface of the particle and, if they are not recombined, they can participate in reactions that involve electron donor and electron acceptor molecules [29].

Since Nb<sub>2</sub>O<sub>5</sub> has a band gap of about 3.4 eV, suitable for a desired photocatalytic effect in the moderate UV region, the investigation of Nb<sub>2</sub>O<sub>5</sub> as a photocatalyst is currently receiving a lot of attention. Prado *et al.* [30] investigated the photodegradation of indigo carmine dye, widely used as a textile colouring agent, using Nb<sub>2</sub>O<sub>5</sub>. The results indicate that almost 100% of dye degradation occurred at 90 minutes after placing it in the niobium pentoxide system. An interesting study was carried out by Oliveira *et al.* [31] using mass spectroscopy (ESI-MS). The results showed that Nb<sub>2</sub>O<sub>5</sub> was a good catalyst for oxidizing organic compounds and that this catalytic activity was favoured when the synthesized niobia was pretreated with hydrogen peroxide. The photocatalytic efficiency of Nb<sub>2</sub>O<sub>5</sub> was increased by modifying it, either by doping with active metals or manufacturing composites and mixed oxides. In this way MnO<sub>2</sub>-loaded Nb<sub>2</sub>O<sub>5</sub>/carbon clusters were formed [32] for the reduction of methylene blue, Nb<sub>2</sub>O<sub>5</sub>-TiO<sub>2</sub> compounds were prepared for an effective photocatalytic treatment of the vinasse [33]. To promote photocatalytic activity of niobium pentoxide in the presence of visible light, meanwhile, nanostructures of Nb<sub>2</sub>O<sub>5</sub> were formed by modifying it mainly with carbon or nitrogen [34,35]. Without any doubt, the synthesis method used to obtain Nb<sub>2</sub>O<sub>5</sub> affects the photocatalytic activity of this oxide as indicated by the works of Raba *et al.* [36] and Li *et al.* [37].

In this study, Nb<sub>2</sub>O<sub>5</sub> powders were synthesized by the controlled precipitation method using aqueous solutions

of ammonium niobate oxyhydrate, ammonium hydroxide as precipitant and water and a water-acetic acid mixture (50 : 50) as solvents. Based on potentiometric titration curves, the different stages of the synthesis method were determined. The physicochemical processes that could occur during the addition of the precipitant were analysed, paying special attention to the system that used water as a solvent. The obtained ceramic powders were characterized using different techniques, taking particular note of the sample that showed the highest photocatalytic activity.

## II. Experimental procedure

### 2.1. Synthesis of Nb<sub>2</sub>O<sub>5</sub> nanoparticles

Nb<sub>2</sub>O<sub>5</sub> was synthesized from ammonium niobate oxyhydrate (NH<sub>4</sub>)<sub>2</sub>[NbO(C<sub>2</sub>O<sub>4</sub>)<sub>3</sub>] · 3 H<sub>2</sub>O using controlled precipitation method. Before obtaining the niobium pentoxide, the potentiometric titration curve was recorded to determine the pH at which the sample would be synthesized. These curves were obtained by recording simultaneously the amount of added ammonium hydroxide (1 ml/min), and pH of the system.

The synthesis was started with preparation of 0.2 M solution by dissolving (NH<sub>4</sub>)<sub>2</sub>[NbO(C<sub>2</sub>O<sub>4</sub>)<sub>3</sub>] · 3 H<sub>2</sub>O in 100 ml of water or in 100 ml of a 50 : 50 mixture of water and acetic acid. Ammonium hydroxide (NH<sub>4</sub>OH, Mallinckrodt 28–30%) was then added, keeping the addition rate and addition volume constant. Continuous stirring was maintained until the required pH values in the solution (determined from potentiometric titration) were obtained: ~5.0 and ~7.1 with water and ~5.0 and ~9.0 with mixture of water and acetic acid solvent. The slurry was then dried using a Buchi B-169 rota-evaporator at a temperature of 100 °C for the water solvent, or 120 °C if the water-acetic acid was used. Finally, the obtained dry powders were heat treated at 400, 500 and 600 °C for 2 h using an oven (Thermolyne).

### 2.2. Characterization of solids

The dried or heat treated powders were macerated in an agate mortar and characterized using FTIR and Raman spectroscopy, XRD and TEM. XRD patterns of the powder were measured in a D2 Phaser diffractometer (Bruker) providing X-rays with a wavelength of 1.5418 Å. Transmission electron microscopy (TEM) images were taken using a JEOL-2010 electron microscope with an accelerating voltage of 200 kV; some HR-TEM images were taken using a JEM ARM 200 CF spectrometer. Fourier transform infrared (FTIR) spectra were taken on a Perkin Elmer Spectrum One spectrometer.

### 2.3. Photodegradation test

In order to determine the characteristics of the dye (methylene blue, C<sub>16</sub>H<sub>18</sub>N<sub>3</sub>ClS) adsorption equilibrium on the synthesized niobium pentoxide, the adsorption study was carried out. For this purpose, 10 mg of each

of the synthesized powders were taken and dispersed in 100 ml of solution of methylene blue with concentration of 50 ppm, under continuous stirring, at pH 6.9 and room temperature in complete darkness. Subsequently, every 10 min, aliquots of this suspension were removed and spectra of these were taken, taking account of the maximum absorbance shown by the methylene blue at 665 nm, using an UV-visible spectrophotometer (Spectronic Genesys 6). This procedure was repeated until 60 minutes of assay were completed. It should be noted that most photocatalytic tests performed by other groups [38,39] commonly use low concentrations, of 3 and 10 ppm up to 50 ppm, and volumes of no more than 10 ml. Finally, using calculations and the calibration curve method [40], the mass of methylene blue adsorbed on the solids was determined. The coefficient  $q$  (mg methylene blue adsorbed/mg photocatalyst) was plotted versus time to determine the amount of time to maintain the system under continuous stirring before turning on the UV lamp. Thus, it was possible to determine more accurately the photo-degradation capacity of the suspended niobium solids without it being masked by the adsorption that can occur on the solids present in the system.

To determine the photo-degradation capacity of the synthesized solids, 100 ml of aqueous methylene blue solution having a concentration of 50 ppm was poured into a 250 ml beaker. Next, 10 mg of the synthesized  $\text{Nb}_2\text{O}_5$  powders were weighed and added to the corresponding methylene blue solution. Each mixture was taken to a “solar simulator” built in the laboratory, stirred previously for the time determined from the adsorption kinetic curves of each in order to eliminate, or minimize, the effect of the adsorption. Following the specific stirring time for each sample, the suspension was placed inside the simulator and visible light lamps were turned on using full simulated solar light (FSS) with 1.300 lx intensity to start the photodegradation test.

During the photo-degradation process, the system was maintained under continuous stirring, at 500 rpm, and every 5 min aliquots of this suspension were taken to determine the photodegradation effect. These samples were placed in a quartz cell and placed in the UV-visible spectrophotometer to obtain the absorbance value of the system at a wavelength of 665 nm. After taking the ab-

sorbance, the suspension was poured into the beaker again. This process was repeated every 5 min during first 20 minutes and then every 10 min for the rest 40 minutes. Finally, the percentage of degradation of methylene blue was plotted versus time. The same steps were followed for the photolysis testing but in this case only the methylene blue solution was used.

### III. Results and discussion

#### 3.1. Potentiometric titration

Figure 1 shows the potentiometric titration curves corresponding to the  $(\text{NbO}(\text{C}_2\text{O}_4)_2)\text{-H}_2\text{O}\text{-NH}_4\text{OH}$  and  $(\text{NbO}(\text{C}_2\text{O}_4)_2)\text{-H}_2\text{O}\text{-CH}_3\text{COOH}\text{-NH}_4\text{OH}$  systems, with precursor concentration of 0.2 M (for the other precursor concentrations the titration curves were similar and no significant changes were recorded).

In the system with the mixture of water and acetic acid (Fig. 1b), it was observed that the first region is quite extensive since a large amount of ammonium hydroxide is needed to neutralize the strong effect of the acetic acid, whose pH is very low. Moreover, considering that acetic acid is a weak acid, during addition of a base a buffer effect is created at around pH = 4.7, which then requires a high consumption of ammonium hydroxide in order to see representative changes in the pH of the system. Furthermore, considering that there are  $\text{NH}_4^+$  ions from the precursor in the solution, when  $\text{NH}_4\text{OH}$  is added it generates a shift of the equilibrium of the reaction  $\text{NH}_3 + \text{H}_2\text{O} \longrightarrow \text{NH}_4\text{OH}$  to the left, towards the formation of ammonia, whose release in the process of synthesis is evident.

The similar behaviour was observed with water as solvent (Fig. 1a). However, there is no high consumption of ammonium hydroxide because only the precursor and water are present in the solution. In the system with distilled water, Fig. 1a, there could clearly be distinguished three regions where the consumption of  $\text{OH}^-$  by the system is appreciable. The difference in the shape of the titration curves, presented in Figs 1a,b, is due to the different natures of the solvents, indicating that the chemical reactions that occur within each of the system are different. Taking into account the changes in the titration curves, different pH values were defined for carrying out the synthesis of the  $\text{Nb}_2\text{O}_5$ : in the case of

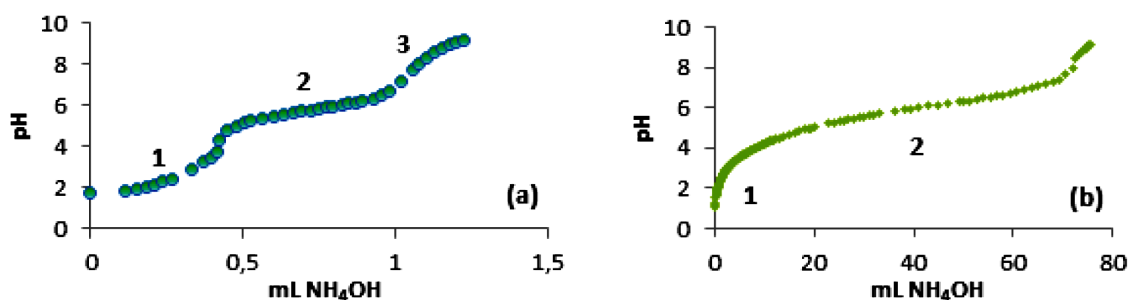


Figure 1. Potentiometric titration curves for 0.2 M solution of niobium oxalate prepared using: a) distilled water and b) acetic mixture of water and acetic acid as solvents

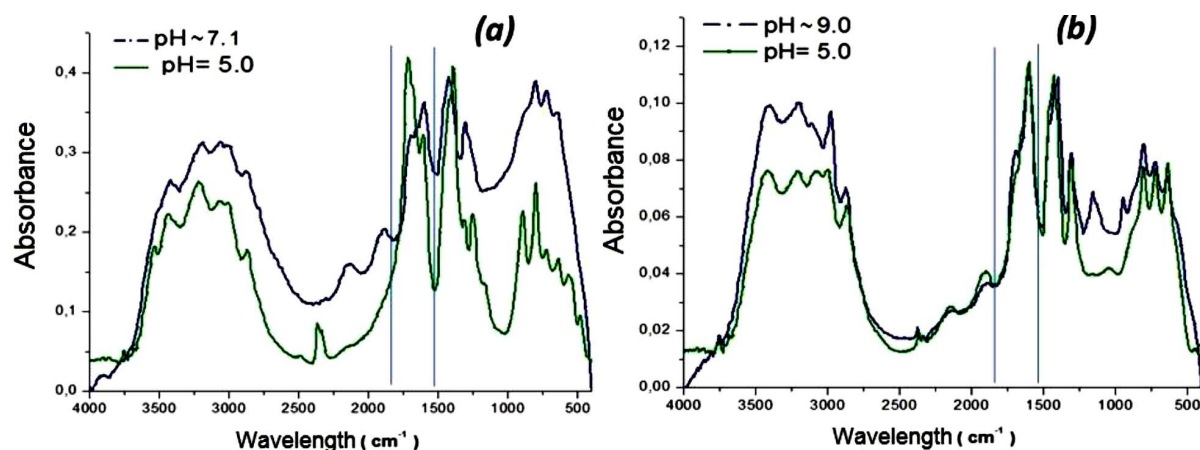


Figure 2. FTIR spectra corresponding to the precipitate obtained (a) in the water solvent, dried at 100 °C, and (b) in the acetic acid solvent, dried at 120 °C

water, pH values of ~5.0 and ~7.1 were taken, while 5.0 and ~9.0 were used for the system containing acetic acid.

### 3.2. Characterization of dried powders

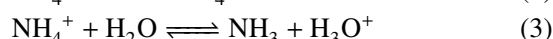
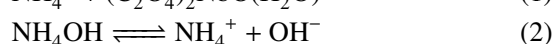
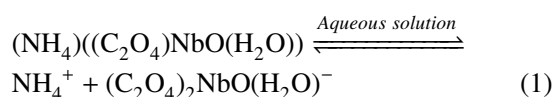
FTIR spectra of the solid samples synthesized and dried at 100 °C for the water solvent and 120 °C for the acetic acid solvent are presented in Figs. 2a and 2b, respectively. In all of them, a band was observed around  $\sim 806\text{ cm}^{-1}$  attributed to the  $\delta(\text{COO})$  vibrational mode and one at  $\sim 1700\text{ cm}^{-1}$  corresponding to  $V_{as}(\text{CO})$  coming from the bidentate oxalate ligand [41]. The band observed at  $\sim 3425\text{ cm}^{-1}$  shows the presence of N–H bonds, indicating a strong presence of amino functional groups in the precipitate. Table 1 shows the assignation of Nb-related functional groups to the bands seen in the spectra in Fig. 2.

In order to analyse more closely the FTIR spectra (Fig. 2) obtained for the synthesized solid samples, deconvolution in the region  $400\text{--}1000\text{ cm}^{-1}$  was carried out using the FITYK software. In Fig. 3, bands characteristic for the niobium-oxygen bond can be seen, such as the band between  $600\text{--}700\text{ cm}^{-1}$ , corresponding to angular vibrations of Nb–O–Nb, another at  $\sim 880\text{ cm}^{-1}$ , corresponding to stretches of the Nb–O and the band located around  $\sim 950\text{ cm}^{-1}$  that might be associated with surface Nb=O stretches [43–45]. Although the data are not shown, the integrated area was calculated for the band between 600 and  $700\text{ cm}^{-1}$  and the results showed

an increasing tendency of Nb–O–Nb peak intensity as the pH of the system increased, indicating that the presence of large quantities of  $\text{OH}^-$  groups in the system would strengthen the Nb–O–Nb bond.

### 3.3. Proposed mechanism of $\text{Nb}_2\text{O}_5$ formation

Based on the FTIR results, a mechanism for the decomposition of the ammonium oxalate precursor during the addition of  $\text{NH}_4\text{OH}$  and formation of  $\text{Nb}_2\text{O}_5$  is proposed (Fig. 4). The mechanism can be expressed through a series of chemical reactions that may occur during the different stages of formation of the solid within the aqueous solution, during both dissolution of the precursor and addition of the precipitant ( $\text{NH}_4\text{OH}$ ). The first stage is the dissolution of the niobium ammonium oxalate, which can be expressed through the following reaction:



With the addition of ammonia to the solution, the following reactions would be favoured:

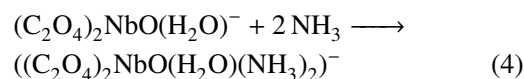


Table 1. Main FTIR spectrum bands associated with vibrational modes of  $\text{Nb}_2\text{O}_5$

Functional group	$\text{cm}^{-1}$	Type of vibration
Nb–O–Nb	600–700	Angular vibrations
Nb=O	948–951	Surface Nb=O stretches
Nb–O	923	Stretching vibrations of Nb–O of $\text{NbO}_6$ units
Nb–O	880	
Nb–OH	3530	Angular vibrations
Nb–N	$\sim 195$	Asymmetric vibrations
Nb–N	$\sim 412$	Asymmetric vibrations
Nb–O–C	3400 and 3500	—

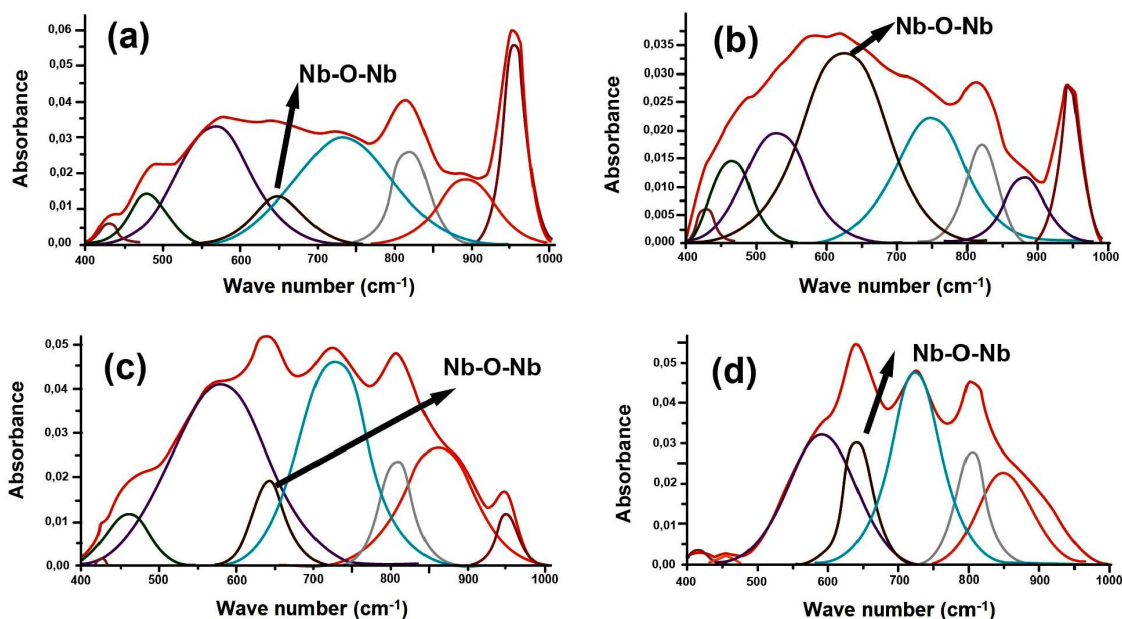
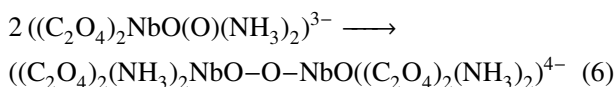
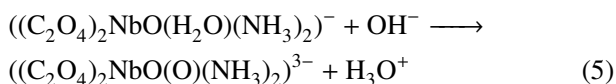


Figure 3. Deconvolution of IR spectrum, between 400 cm<sup>-1</sup> and 1000 cm<sup>-1</sup>, corresponding to the precipitate obtained in water solvent and dried at 100 °C: a) pH ~5.0 and b) pH ~7.1, and in acetic acid, dried at 120 °C: c) pH ~5.0 and d) pH ~9.0



The incorporation of amino groups in the structure of the complex arises due to the excess NH<sub>4</sub>OH present in the solution, since this was used as precipitating agent. The displacement of the oxalates by amino groups is because the amino groups have a greater chelating effect than the oxalates, so that the latter are able to be displaced. This effect is seen in the FTIR spectra since, as the amount of NH<sub>4</sub>OH is increased, the bands associ-

ated with Nb–N begin to appear. Furthermore, as shown in the diffractogram in Fig. 5, the crystalline structure of the precipitate showed substantial changes with respect to the initial precursor, indicating that the addition of the precipitating agent modified the sphere of coordination of the metal, mainly the bands associated with monodentate type oxalate (see Fig. 2a), as indicated by the above reactions and illustrated in the mechanism in Fig. 4.

By increasing the pH, the hydroxylation of the niobium complexes that would be formed in the system is favoured, as expressed by the following reactions:

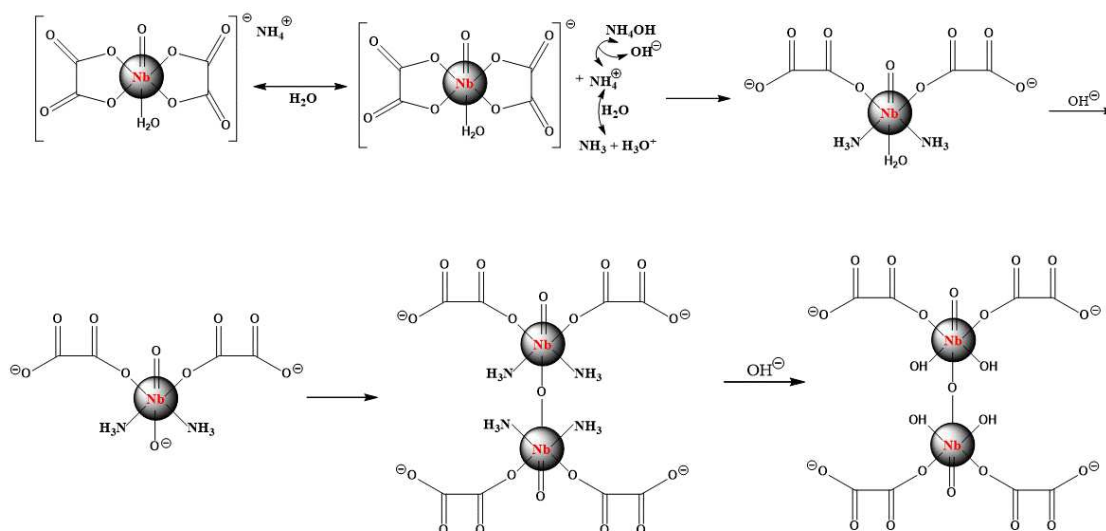
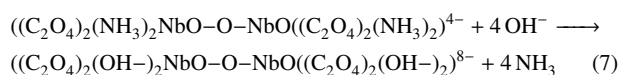


Figure 4. Mechanism proposed to explain the formation of Nb<sub>2</sub>O<sub>5</sub> within water

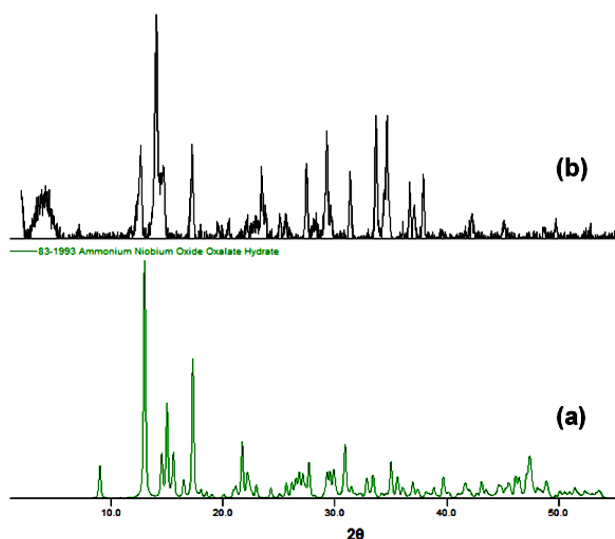


Figure 5. X-ray diffractograms corresponding to: a) ammonium niobium oxalate (precursor) and b) precipitate obtained in the system with water and dried at 100 °C

While the hydroxyl is not a better chelator than the amino group, it is possible that the formed complexes generated with the hydroxyls are more stable than with the amino groups. It should further be taken into account that, as pH is increased, the amount of  $\text{OH}^-$  in solution increases and encourages the displacement of the amino groups by the hydroxyls as a result of being present in greater quantities.

### 3.4. Characterization of calcined powders

The FTIR spectra of the calcined powders at 600 °C (Fig. 6) show that the most important bands are between 400 and 1000  $\text{cm}^{-1}$  associated with the functional groups from bonds between Nb and oxygen and/or OH (Table 1). A band can be seen between 1500 and 1700  $\text{cm}^{-1}$  which is associated with water adsorbed on the surface of the  $\text{Nb}_2\text{O}_5$ . Figure 7 shows the deconvoluted IR spectra, between 400 and 1000  $\text{cm}^{-1}$ , corresponding to the samples heat treated at 600 °C for the solid obtained in both water (Figs. 7a and 7b) and acetic acid (Figs. 7c and 7d). It can be seen that in this region bands as-

sociated with mainly the Nb–O and Nb–OH bonds are observed, including those of Nb–O–Nb angular vibrations, in the range 600–700  $\text{cm}^{-1}$ , which vary according to the conditions of synthesis: for water as solvent between 690 and 664  $\text{cm}^{-1}$  and for acetic acid between 696 and 675  $\text{cm}^{-1}$ ; depending on the pH, bands are displaced with respect to that shown for commercial niobium pentoxide (653  $\text{cm}^{-1}$ ). Figure 7 highlights the effect of both the synthesis pH and the solvent used on the local structure of the  $\text{Nb}_2\text{O}_5$  obtained.

In order to learn more about the sample that showed the best photo-degradation response (as discussed later in the article, this was the one synthesized in acetic acid, pH ~9.0 and thermally treated at 600 °C), its Raman spectrum was measured (Fig. 8). The band at around 700  $\text{cm}^{-1}$  corresponds to the symmetric stretching modes of the  $[\text{NbO}_6]$  and  $[\text{NbO}_7]$  polyhedra present in an orthorhombic  $\text{Nb}_2\text{O}_5$  [45]. The group of bands located in the lower region of the Raman spectrum, 150–350  $\text{cm}^{-1}$  corresponds to the stretching modes of Nb–O–Nb. In the Raman spectra obtained for other studied samples, which are not shown in this work, no major changes were seen in the band shapes or their location.

Figure 9 shows the X-ray diffractograms obtained for  $\text{Nb}_2\text{O}_5$  synthesized using acetic acid as solvent at pH ~9.0 and treated at different calcination temperatures. These diffractograms show that with the increase in temperature the characteristic peaks of  $\text{Nb}_2\text{O}_5$  became more evident and the samples presented higher crystallization. Specifically, the sample treated at 600 °C showed only crystalline phase niobium pentoxide. By analysing the diffractogram in Fig. 9c it is found that these powders, synthesized by the controlled precipitation method in acetic acid at pH ~9.0, showed a mixture of crystalline phases, the orthorhombic (PDF 01-071/0336) being the most important and monoclinic (PDF 27-1312) as the minority phase [46]. The crystalline planes (001) and (180) correspond to diffraction peaks detected at  $2\theta$  of 22.6° and 28.3° belonging to the orthorhombic phase [42]. Although the diffractograms of the other samples synthesized in this work are not displayed, they showed a similar behaviour to that of Fig. 9; moreover, the diffractogram of this specific sample (synthesized in

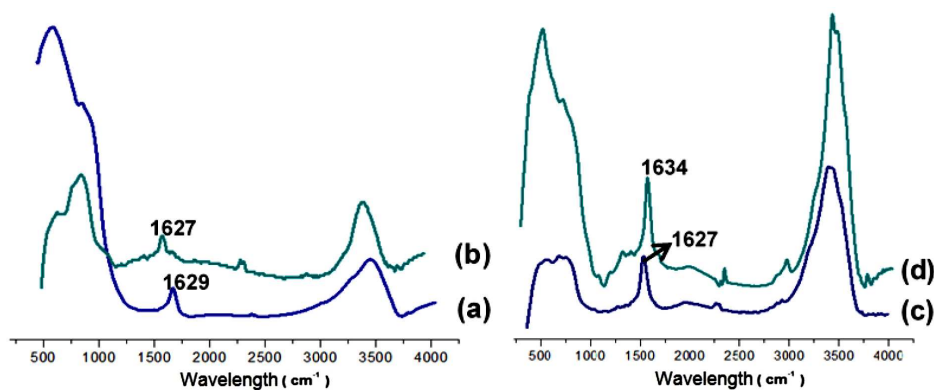


Figure 6. IR spectra for powders calcined at 600 °C obtained from the acetic acid solvent system: a) pH ~9.0 and b) pH ~5.0, and with water as solvent: c) pH ~5.0 and d) pH ~7.1

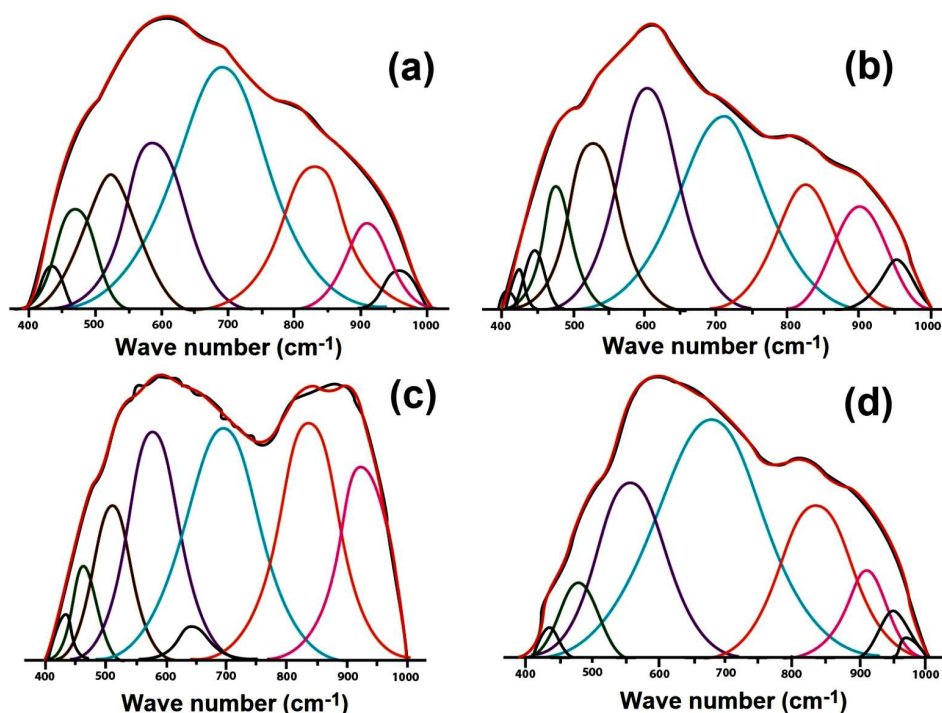


Figure 7. Deconvolutions between 400-1000  $\text{cm}^{-1}$  of the IR spectra for samples calcined at 600 °C of solids synthesized in acetic acid solvent system: a) pH  $\sim$ 9.0 and b) pH  $\sim$ 5.0, and with water as solvent: c) pH  $\sim$ 5.0 and d) pH  $\sim$ 7.1

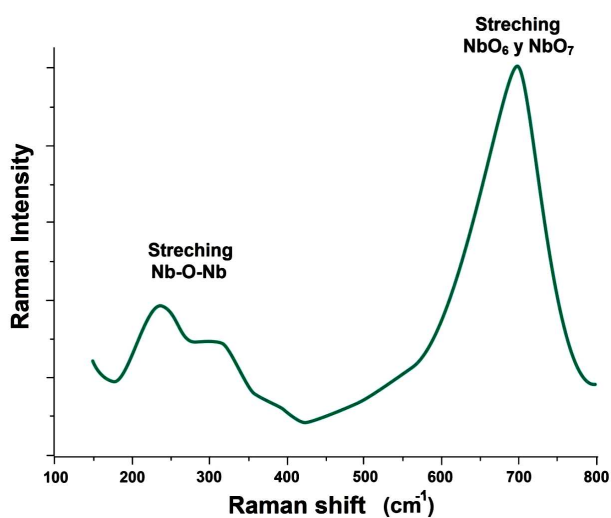


Figure 8. Raman spectra of a sample thermally treated at 600 °C that was synthesized at pH  $\sim$ 9.0, using acetic acid as solvent

acetic acid, pH  $\sim$ 9.0 and treated at 600 °C) is of interest because, as it will be seen later on, it showed the greatest photo-degradation effect.

The effect of changes in synthesis conditions – the nature of the synthesis solvent and/or working pH – was demonstrated markedly in the morphology and particle size of the obtained solids heat-treated at 600 °C, as can be seen in the transmission electron micrographs in Fig. 10. For the samples synthesized in water at pH  $\sim$ 7.1, Fig. 10a, the particles were dispersed and had a spheroidal morphology, while using the same solvent, but at pH  $\sim$ 5.0, the primary particles were agglomerated, took the shape of small tablets and their

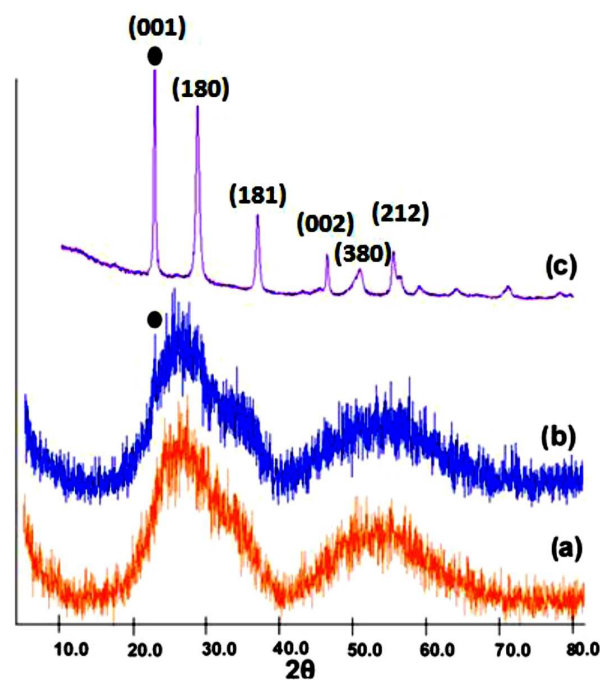


Figure 9. XRD patterns corresponding to samples synthesized using acetic acid as solvent, at pH of  $\sim$ 9.0 and calcined at: a) 400 °C, b) 500 °C and c) 600 °C

size was  $>$ 50 nm, thus larger than those obtained at pH  $\sim$ 7.1 ( $<$ 50 nm). When acetic acid was used as a solvent for synthesis, the primary particles synthesized at pH  $\sim$ 5.0 formed loose agglomerates, with diameter  $>$ 500 nm (Fig. 10c), while those obtained at pH  $\sim$ 9.0 formed agglomerates with a very particular texture, as shown in Fig. 10d.

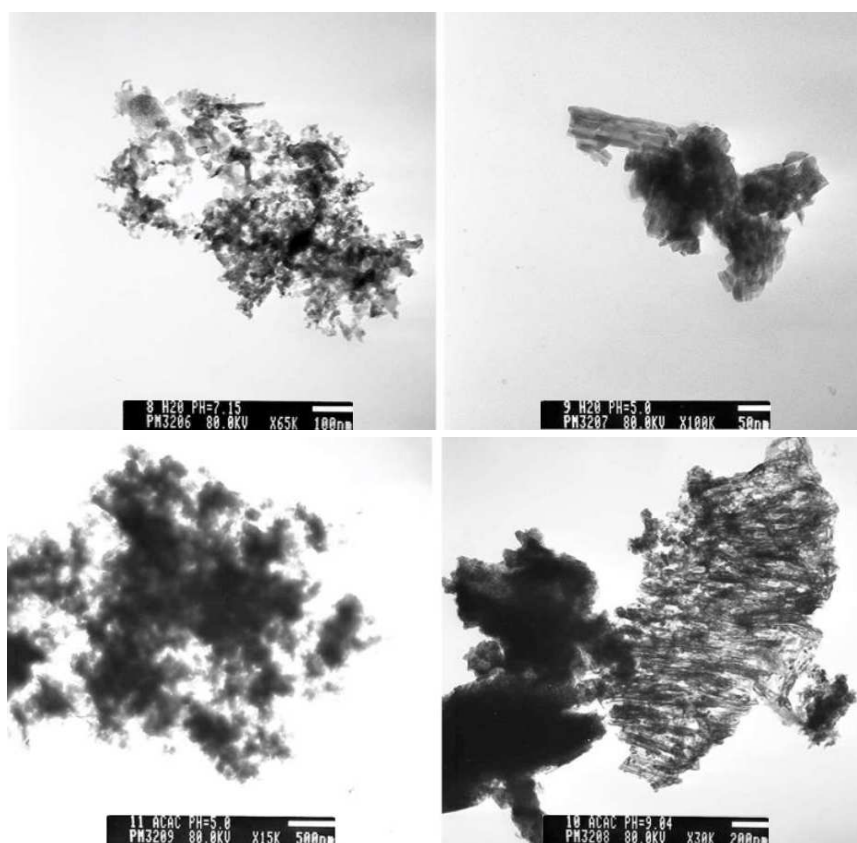


Figure 10. TEM micrographs corresponding to ceramic powders synthesized using water as solvent at: a) pH ~7.1 and b) pH ~5.0; and acetic acid at c) pH ~5.0 and d) pH ~9.0, heat treated to 600 °C

Since this latter solid was the sample that showed the best photodegradation response, as will be shown later, a photographic record was made of it (see Fig. 11). As the images show, there is a marked difference in particle size and in their texture and morphology, according to the value of calcination temperature. For the sample calcined at 400 °C, Fig. 11a, large agglomerates are observed, without a defined morphology, while on treating the solid at 500 °C a fibrous texture can be seen (Fig. 11b). After the treatment at 600 °C, Fig. 11c, the primary particles had a morphology in the form of

tablets, with a particle size <100 nm, with a special texture (more evident in Fig. 10d). These presented differences in texture and morphology, mainly the solids synthesized in acetic acid, can be justified considering that both the synthesis solvent and the Nb precursor  $(\text{NH}_4)_2\text{H}_2[\text{NbO}(\text{C}_2\text{O}_4)_3] \cdot 3 \text{H}_2\text{O}$  were organic in nature. This condition caused that organic species of the solvent and/or those formed during the reaction, played a role of the capping agents, which bind to the particle surface and thus limit the crystal growth and influence particle morphology as well as assembly behaviour [47].

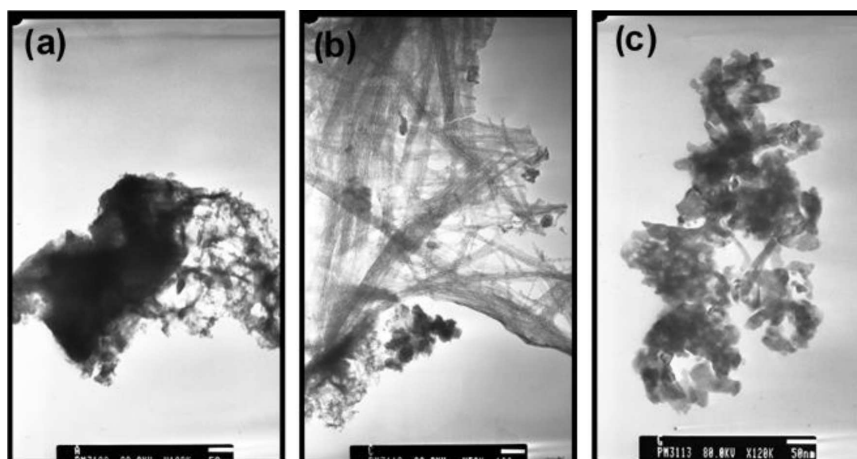


Figure 11. TEM micrographs of ceramic powders obtained at pH ~9.0 using acetic acid as solvent and heat treated at: a) 400 °C, b) 500 °C and c) 600 °C

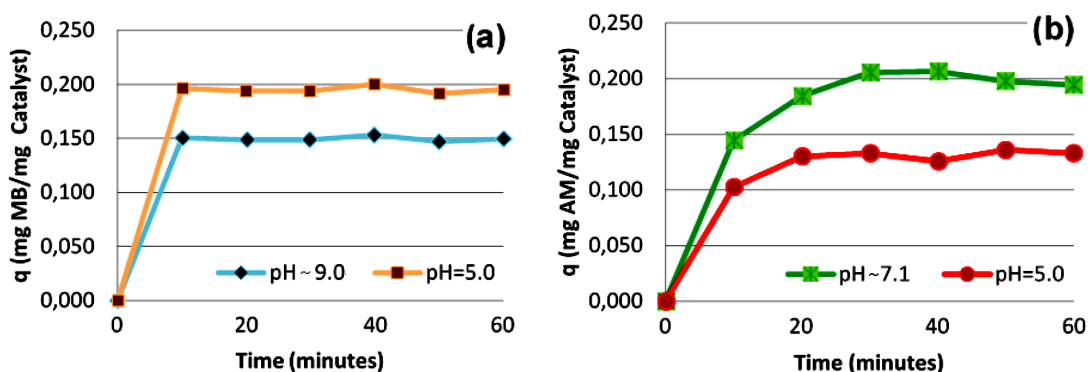


Figure 12. Curves of the adsorption of methylene blue (MB), in the dark, corresponding to solids synthesized in: a) acetic acid and b) water, for different pH

### 3.5. Photocatalytic activity of $Nb_2O_5$ nanoparticles

Figure 12 shows the adsorption curves obtained for different synthesized solids of niobium pentoxide, varying the conditions of synthesis. The solids synthesized in acetic acid were seen to reach the adsorption-desorption equilibrium with the dye more rapidly than when water was used as the solvent for synthesis. This indicates that the surface interaction that occurred between the dye and the solid synthesized in acetic acid (Fig. 12a) was stronger than that for the solid obtained in water (Fig. 12b). As a result, the speed of adsorption was greater for the solid synthesized in acetic acid, as the curves indicate.

Meanwhile, considering the effect of the pH of synthesis for both solvents on dye adsorption by the solids, it was observed that the behaviour does not follow the same trend. With acetic acid, the particles obtained at an acidic pH showed a higher adsorption, while for the solids synthesized in water, those that had a higher adsorption were the samples obtained at pH > 7. Comparing the adsorption curves of the powders synthesized in this work (Fig. 12) it can be seen that the solid with a slightly greater efficiency in adsorbing methylene blue is that synthesized in water at pH ~7.1, possibly due to its uniformity in particle size and particle morphology (Fig. 10a).

The photo-degradation effect of the  $Nb_2O_5$  powders obtained in this work was affected significantly by variation of the solvent and the pH of synthesis, as seen in Fig. 13. The highest photo-degradation capacity was shown for the solid synthesized at a basic pH value, ~9.0, with acetic acid as solvent, with a percentage degradation of 59.8% after 60 minutes. For solids also synthesized in acetic acid but at acidic pH values, for example ~5.0, the percentage degradation was lower, 50.8%. For the solids synthesized in water, a percentage degradation of 50.3% was found for the sample obtained at pH ~7.1 and 46.5% for the solid synthesized at pH ~5. Thus, independent of the synthesis solvent, the solids that had the best photo-degradation capacity were obtained at pH > 7.

Comparing the results of the photo-degradation of methylene blue, Fig. 13, with those of the adsorption

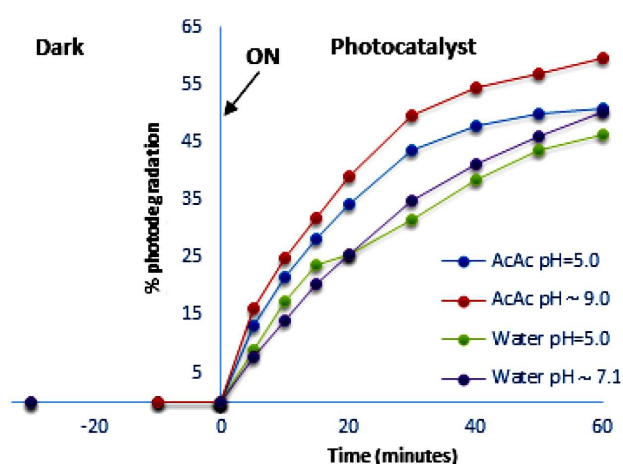
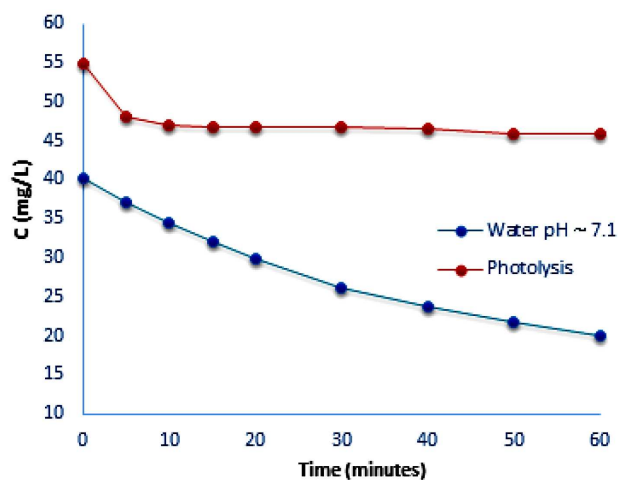


Figure 13. Percentage degradation of methylene blue, as a function of irradiation time, caused by niobium pentoxide obtained by varying some synthesis parameters

curves, Fig. 12, the solids synthesized in water show the same trend in photo-degradation (Fig. 13) as found for the adsorption (Fig. 12b), i.e. the sample that showed the highest capacity for adsorbing the dye also showed the highest photo-degradation capacity (solid synthesized at pH ~7.1). This was not the case for the samples synthesized in acetic acid, where the solid that had the highest adsorption capacity (obtained at pH ~5, Fig. 12a), had the lowest photo-degradation effect (Fig. 13).

Independent of its synthesis method, the addition of  $Nb_2O_5$  to the methylene blue solution clearly degraded the dye to a greater or lesser degree (Fig. 13). Figure 14 compares the degradation of methylene blue caused by the action of radiation, photolysis, to that prompted by the solid sample synthesized in water at pH ~7.1, which had obvious degradation effect, demonstrating that the presence of the oxide increases the degradation of the dye. It should be noted that none of the  $Nb_2O_5$  powders synthesized in this work degraded methylene blue 100% within the 60 minutes of exposure to UV radiation. However, it must be taken into account that the photocatalytic tests reported in the literature use maximum concentrations of methylene blue of 10 ppm in volumes of 100 ml [48,49] or 50 ppm in 10 ml, while in this study a concentration of 55 ppm was used, taking a



**Figure 14.** Degradation of methylene blue via photolysis and photocatalysis by means of UV irradiation on slurries containing powders of synthesized  $\text{Nb}_2\text{O}_5$

100 ml solution with the same amount of photocatalyst (10 mg), indicating that the latter would be the more effective.

In this work synthesized samples showed differences in photocatalytic activity (Fig. 13), evidencing the importance of the conditions of synthesis, the shape and size of the particles and their state of aggregation (texture) in the determination of their functionality, specifically in the photodegradation of the methylene blue. The state of aggregation of the  $\text{Nb}_2\text{O}_5$  nanoparticles (Figs. 10 and 11) is an important factor in the determination of their photocatalytic capacity, as it happens in other systems [50]. This is because the generation of free hydroxyl radicals vary with aggregate structure and size, as predicted by the theory, because the reactivity of these aggregates is reduced when they are large and dense; the aggregation affect the local concentration of one of the key reactants - particle surfaces - which would alter ROS production. On the other hand, the photocatalytic activity of  $\text{Nb}_2\text{O}_5$  nanoparticles is conditioned by the synthesis conditions, nature of the solvent and working pH. In other works the same thing happens, the photocatalytic activity of metal oxide is determined by nature of the solvent which affects the concentration of specific sites (defects) [51].

#### IV. Conclusions

In this study, a methodology of synthesis was structured with the aim of obtaining submicron  $\text{Nb}_2\text{O}_5$  with variations in morphology and size, using ammonium niobate oxyhydrate  $(\text{NH}_4)_2[\text{NbO}(\text{C}_2\text{O}_4)_3] \cdot 3\text{H}_2\text{O}$  as a precursor. The nature of the solvents (water or acetic acid) and the pH of synthesis used for the process are important factors in obtaining  $\text{Nb}_2\text{O}_5$  with the desired physical and chemical characteristics. In niobium pentoxide synthesis using two solvents under consideration and at different working pH values a significant effect was observed, primarily on the morphol-

ogy of the ceramic powders obtained as well as its state of aggregation (texture). After the thermal treatment of the obtained precipitate, between 500 and 600 °C, a good crystallization of the solid was achieved, obtaining the orthorhombic phase ( $\text{T-Nb}_2\text{O}_5$ ) as the only crystalline phase. Furthermore, considering potential applications of  $\text{Nb}_2\text{O}_5$ , the photo-degrading action of particles was tested on the organic molecule, methylene blue. Although niobium pentoxide solids obtained in acetic acid showed an adsorption time for the dye less than those synthesized in water, they displayed greater photo-degradation efficiency, in spite of the spheroidal morphology and smaller particle size of the solids obtained in water.

**Acknowledgement:** This work was performed under project ID 4032, funded by the vice-Rectorate for Research at the University of Cauca (VRI - Universidad del Cauca). We are very grateful to Colin McLachlan for suggestions relating to the English text.

#### References

1. C.-C. Lee, C.-L. Tien, J.-C. Hsu, "Internal stress and optical properties of  $\text{Nb}_2\text{O}_5$  thin films deposited by ion-beam sputtering", *Appl. Opt.*, **41** (2002) 2043–2047.
2. F. Richter, H. Kupfer, P. Schlott, T. Gessner, C. Kaufmann, "Optical properties and mechanical stress in  $\text{SiO}_2/\text{Nb}_2\text{O}_5$  multilayers", *Thin Solid Films*, **389** (2001) 278–283.
3. T. Maruyama, S. Arai, "Electrochromic properties of niobium oxide thin films prepared by radio frequency magnetron sputtering method", *Appl. Phys. Lett.*, **63** (1993) 869–870.
4. M.E. Gimon-Kinsel, K.J. Balkus, "Pulsed laser deposition of mesoporous niobium oxide thin films and application as chemical sensors", *Micropor. Mesopor. Mater.*, **28** (1999) 113–123.
5. M. Niederberger, G. Garnweitner, N. Pinna, G. Neri, "Non-aqueous routes to crystalline metal oxide nanoparticles: Formation mechanisms and applications", *Prog. Solid State Chem.*, **33** (2005) 59–70.
6. S. V Ryabtsev, A. V Shaposhnick, A.N. Lukin, E.P. Domashevskaya, "Application of semiconductor gas sensors for medical diagnostics", *Sensors Actuat. B Chem.*, **59** (1999) 26–29.
7. P. Carniti, A. Gervasini, M. Marzo, "Dispersed  $\text{NbO}_x$  catalytic phases in silica matrixes: influence of niobium concentration and preparative route", *J. Phys. Chem. C.*, **112** (2008) 14064–14074.
8. M.A. Aegerter, "Sol-gel niobium pentoxide: a promising material for electrochromic coatings, batteries, nanocrystalline solar cells and catalysis", *Sol. Energy Mater. Sol. Cells*, **68** (2001) 401–422.
9. K. Tanabe, "Niobic acid as an unusual acidic solid material", *Mater. Chem. Phys.*, **17** (1987) 217–225.
10. K. Tanabe, "Application of niobium oxides as catalysts", *Catal. Today*, **8** (1990) 1–11.
11. J.L.G. Fierro, *Metal Oxides: Chemistry and Applications*, CRC press, Boca Ratón, 2005.
12. V.S. Braga, F.A. da C. Garcia, J.A. Dias, S.C.L. Dias, "Phase transition in niobium pentoxide supported on silica-alumina", *J. Therm. Anal. Calorim.*, **92** (2008) 851–

- 855.
13. A. Le Viet, M. V Reddy, R. Jose, B.V.R. Chowdari, S. Ramakrishna, "Nanostructured Nb<sub>2</sub>O<sub>5</sub> polymorphs by electrospinning for rechargeable lithium batteries", *J. Phys. Chem. C*, **114** (2009) 664–671.
  14. E.M. Kuznetsova, L.A. Reznichenko, O.N. Razumovskaya, L.A. Shilkina, "The polymorphism of niobium pentoxide and the properties of alkali metal niobates for ferroelectric piezoceramics", *Tech. Phys. Lett.*, **27** (2001) 189–192.
  15. H. Schäfer, R. Gruehn, F. Schulte, "The modifications of niobium pentoxide", *Angew. Chemie Int. Ed.*, **5** (1966) 40–52.
  16. R. Brayner, F. Bozon-Verduraz, "Niobium pentoxide prepared by soft chemical routes: morphology, structure, defects and quantum size effect", *Phys. Chem. Chem. Phys.*, **5** (2003) 1457–1466.
  17. Y. Zhao, X. Zhou, L. Ye, S.C.E. Tsang, "Nanostructured Nb<sub>2</sub>O<sub>5</sub> catalysts", *Nano Rev.*, **3** (2012) 17631.
  18. E.R. Leite, C. Vila, J. Bettini, E. Longo, "Synthesis of niobia nanocrystals with controlled morphology", *J. Phys. Chem. B*, **110** (2006) 18088–18090.
  19. N. Pinna, M. Antonietti, M. Niederberger, "A novel non-aqueous route to V<sub>2</sub>O<sub>5</sub> and Nb<sub>2</sub>O<sub>5</sub> nanocrystals", *Colloids Surfaces A*, **250** (2004) 211–213.
  20. G. Falk, M. Borlaf, T. Bendo, A.P. Novaes de Oliveira, J. Batista Rodrigues Neto, R. Moreno, "Colloidal sol-gel synthesis and photocatalytic activity of nanoparticulate Nb<sub>2</sub>O<sub>5</sub> sols", *J. Am. Ceram. Soc.*, **99** [6] (2016) 1968–1973.
  21. M. Ristić, S. Popović, S. Musić, "Sol-gel synthesis and characterization of Nb<sub>2</sub>O<sub>5</sub> powders", *Mater. Lett.*, **58** (2004) 2658–2663.
  22. F. Hashemzadeh, R. Rahimi, A. Gaffarinejad, "Photocatalytic degradation of methylene blue and Rhodamine B dyes by niobium oxide nanoparticles synthesized via hydrothermal method", *Int. J. Appl. Chem. Sci. Res.*, **1** (2013) 95–102.
  23. O.F. Lopes, E.C. Paris, C. Ribeiro, "Synthesis of Nb<sub>2</sub>O<sub>5</sub> nanoparticles through the oxidant peroxide method applied to organic pollutant photodegradation: A mechanistic study", *Appl. Catal. B Environ.*, **144** (2014) 800–808.
  24. L.A. Rodrigues, M.L.C.P. da Silva, "Synthesis of Nb<sub>2</sub>O<sub>5</sub> · nH<sub>2</sub>O nanoparticles by water-in-oil microemulsion", *J. Non. Cryst. Solids*, **356** (2010) 125–128.
  25. A. Esteves, L.C.A. Oliveira, T.C. Ramalho, M. Goncalves, A.S. Anastacio, H.W.P. Carvalho, "New materials based on modified synthetic Nb<sub>2</sub>O<sub>5</sub> as photocatalyst for oxidation of organic contaminants", *Catal. Commun.*, **10** (2008) 330–332.
  26. B. Zielińska, J. Sreńscek-Nazzal, R. Kaleńczuk, "Photocatalytic hydrogen generation over alkali niobates in the presence of organic compounds", *Polish J. Chem. Technol.*, **10** (2008) 1–3.
  27. P.A.K. Reddy, P.V.L. Reddy, E. Kwon, K.-H. Kim, T. Akter, S. Kalagara, "Recent advances in photocatalytic treatment of pollutants in aqueous media", *Environ. Int.*, **91** (2016) 94–103.
  28. U. Gaya, *Heterogeneous Photocatalysis Using Inorganic Semiconductor Solids*, Springer Science & Business Media, 2013.
  29. C. Karunakaran, R. Dhanalakshmi, "Selectivity in photocatalysis by particulate semiconductors", *Open Chem.*, **7** (2009) 134–137.
  30. A.G.S. Prado, L.B. Bolzon, C.P. Pedroso, A.O. Moura, L.L. Costa, "Nb<sub>2</sub>O<sub>5</sub> as efficient and recyclable photocatalyst for indigo carmine degradation", *Appl. Catal. B Environ.*, **82** (2008) 219–224.
  31. L.C.A. Oliveira, T.C. Ramalho, M. Gonçalves, F. Cereda, K.T. Carvalho, M.S. Nazzarro, K. Sapag, "Pure niobia as catalyst for the oxidation of organic contaminants: mechanism study via ESI-MS and theoretical calculations", *Chem. Phys. Lett.*, **446** (2007) 133–137.
  32. H. Miyazaki, H. Matsui, T. Kuwamoto, S. Ito, S. Karupuchamy, M. Yoshihara, "Synthesis and photocatalytic activities of MnO<sub>2</sub>-loaded Nb<sub>2</sub>O<sub>5</sub>/carbon clusters composite material", *Micropor. Mesopor. Mater.*, **118** (2009) 518–522.
  33. V.S. Santana, N.R.C.F. Machado, "Photocatalytic degradation of the vinasse under solar radiation", *Catal. Today*, **133** (2008) 606–610.
  34. S. Ge, H. Jia, H. Zhao, Z. Zheng, L. Zhang, "First observation of visible light photocatalytic activity of carbon modified Nb<sub>2</sub>O<sub>5</sub> nanostructures", *J. Mater. Chem.*, **20** (2010) 3052–3058.
  35. B. Hu, Y. Liu, "Nitrogen-doped Nb<sub>2</sub>O<sub>5</sub> nanobelt quasi-arrays for visible light photocatalysis", *J. Alloys Compd.*, **635** (2015) 1–4.
  36. A.M. Raba, J. Barba-Ortega, M.R. Joya, "The effect of the preparation method of Nb<sub>2</sub>O<sub>5</sub> oxide influences the performance of the photocatalytic activity", *Appl. Phys. A*, **119** (2015) 923–928.
  37. W. Li, R. Gao, M. Chen, S. Zhou, L. Wu, "Facile synthesis and unique photocatalytic property of niobium pentoxide hollow spheres and the high optoelectronic performance of their nanofilm", *J. Colloid Interface Sci.*, **411** (2013) 220–229.
  38. P. Justin, P.H.K. Charan, G.R. Rao, "High performance Pt-Nb<sub>2</sub>O<sub>5</sub>/C electrocatalysts for methanol electrooxidation in acidic media", *Appl. Catal. B Environ.*, **100** (2010) 510–515.
  39. L. Li, R. Fu, Q. Liao, L. Ji, "Doping behaviors of NiO and Nb<sub>2</sub>O<sub>5</sub> in BaTiO<sub>3</sub> and dielectric properties of BaTiO<sub>3</sub>-based X7R ceramics", *Ceram. Int.*, **38** (2012) 1915–1920.
  40. D.A. Skoog, F. Holler, A.D.A. Timothy, *Principios de Análisis Instrumental*, McGraw-Hill Interamericana de España, 2001.
  41. K. Nakamoto, K. Nakamoto, *Infrared and Raman Spectra of Inorganic and Coordination Compounds*, Wiley, New York, 1977.
  42. L. Yao, X. Wuhong, Z. Jiupeng, M. Xiangdong, "Fabrication and characterization of three-dimensionally ordered macroporous niobium oxide", *Solid State Sci.*, **11** (2009) 1625–1630.
  43. J.S. Souza, K. Krambrock, M.V.B. Pinheiro, R.A. Ando, S. Guha, W.A. Alves, "Visible-light photocatalytic activity of NH<sub>4</sub>NO<sub>3</sub> ion-exchanged nitrogen-doped titanate and TiO<sub>2</sub> nanotubes", *J. Mol. Catal. A Chem.*, **394** (2014) 48–56.
  44. D. Huang, S. Liao, S. Quan, L. Liu, Z. He, J. Wan, W. Zhou, "Synthesis and characterization of visible light responsive N-TiO<sub>2</sub> mixed crystal by a modified hydrothermal process", *J. Non. Cryst. Solids.*, **354** (2008) 3965–3972.
  45. T. Rojac, M. Kosec, M. Polomska, B. Hilczer, P. Šegedin, A. Bencan, "Mechanochemical reaction in the K<sub>2</sub>CO<sub>3</sub>-Nb<sub>2</sub>O<sub>5</sub> system", *J. Eur. Ceram. Soc.*, **29** (2009) 2999–

- 3006.
46. T. Sreethawong, S. Ngamsinlapasathian, S.H. Lim, S. Yoshikawa, “Investigation of thermal treatment effect on physicochemical and photocatalytic H<sub>2</sub> production properties of mesoporous-assembled Nb<sub>2</sub>O<sub>5</sub> nanoparticles synthesized via a surfactant-modified sol-gel method”, *Chem. Eng. J.*, **215** (2013) 322–330.
  47. M. Niederberger, “Nonaqueous sol-gel routes to metal oxide nanoparticles”, *Acc. Chem. Res.*, **40** (2007) 793–800.
  48. C. Li, Z. Sun, Y. Xue, G. Yao, S. Zheng, “A facile synthesis of g-C<sub>3</sub>N<sub>4</sub>/TiO<sub>2</sub> hybrid photocatalysts by sol-gel method and its enhanced photodegradation towards methylene blue under visible light”, *Adv. Powder Technol.*, **27** (2016) 330–337.
  49. H.R. Mardani, M. Forouzani, M. Ziari, P. Biparva, “Visible light photo-degradation of methylene blue over Fe or Cu promoted ZnO nanoparticles”, *Spectrochim. Acta A*, **141** (2015) 27–33.
  50. D. Jassby, J. F. Budarz, M. Wiesner, “Impact of aggregate size and structure on the photocatalytic properties of TiO<sub>2</sub> and ZnO nanoparticles”, *Environ. Sci. Technol.*, **46** (2012) 6934–6941.
  51. M. Montero-Muñoz, J.E. Ramos-Ibarra, J.E. Rodríguez-Páez, M.D. Teodoro, G.E. Marques, A.R. Sanabria, P.C. Cajas, C.A. Páez, B. Heinrichs, J.A.H. Coaquira, “Role of defects on the enhancement of the photocatalytic response of ZnO nanostructures”, *Appl. Surf. Sci.*, **448** (2018) 646–654.